ACS Photonics

Article

pubs.acs.org/journal/apchd5

Wavelength-Selective Diffraction from Silica Thin-Film Gratings

Ijaz Rashid,[†] Haider Butt,[*,†] Ali K. Yetisen,[‡] Bruno Dlubak,[§] James E. Davies,[†] Pierre Seneor,[§] Aymeric Vechhiola,[§] Faycal Bouamrane,[§] and Stephane Xavier[∥]

[†]Microengineering and Nanotechnology Laboratory, School of Engineering, University of Birmingham, Birmingham B15 2TT, United Kingdom

[‡]Harvard-MIT Division of Health Sciences and Technology, Harvard University and Massachusetts Institute of Technology, Cambridge, Massachusetts 02139, United States

[§]Unité Mixte de Physique, CNRS, Thales, Univ. Paris-Sud, Université Paris-Saclay, Palaiseau 91767, France

[∥]Thales Research and Technology, 91767 Palaiseau, France

S *Supporting Information*

ABSTRACT: A reflective diffraction grating with a periodic square-wave profile will combine the effects of thin-film interference with conventional grating behavior when composed of features having a different refractive index than that of the substrate. A grating period of 700−1300 nm was modeled and compared for both silicon (Si) and silicon dioxide (SiO_2) to determine the behavior of light interaction with the structures. Finite element analysis was used to study nanostructures having a multirefractive index grating and a conventional single material grating. A multimaterial grating has the same diffraction efficiency as that of a grating formed in a single material, but had the advantage of having an ordered relationship between the grating dimensions (thickness and period) and the intensity of reflected and diffracted optical wavelengths. We demonstrate a color-selective feature of the modeled SiO_2 grating by fabricating samples with grating periods of 800 and 1000 nm, respectively. A high diffraction efficiency was measured for the green wavelength region as compared to other colors in the spectrum for 800 nm grating periodicity; whereas wavelengths within the red region of spectrum interfered constructively for the grating with 1000 nm periodicity resulting a higher efficiency for red color bandwidth. The results show that diffraction effects can be enhanced by the thin-film interference phenomenon to produce color selective optical devices.

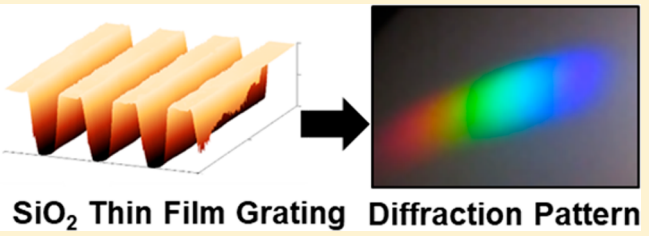

KEYWORDS: *photonics, nanotechnology, diffraction gratings, thin-film interference, color-selective grating*

Diffraction gratings have numerous applications in lasers, holography, optical data storage, light-trapping in solar cells, security holograms, and biosensors.[1−4] They have been utilized for precisely controlling optical beams (e.g., splitting and steering).[5] Light diffracted from nanostructures can create interference effects and diffract narrow-band light.[6] SiO_2 (silica) and TiO_2 (titania) thin films have been previously investigated for optical applications due to their low optical propagation losses.[7−9] SiO_2 has approximately 8× more sensitivity to light as compared to pure Si.[10] Conventional single material reflective gratings can be fabricated using microprocesses such as preferential etching of monocrystalline Si.[11] While single material gratings, which displayed diffraction efficiencies up to 96%, have been developed,[12] investigation of the optical features of multimaterial diffraction gratings has been limited.

In the present work, we studied the optical effects produced by a one-dimensional (1D) reflective diffraction grating based on silica thin films fabricated on Si substrates. We have also compared these optical properties with a grating made of Si on Si substrates. We combined the color-selective properties of thin films with diffraction using a 1D SiO_2 based color-selective grating. Extensive theoretical work exists in the literature concerning thin films and diffraction grating separately. However, combining both concepts to study the distinct behavior of diffraction grating formed from a single thin film has not been demonstrated. Computational modeling was used to determine grating parameters such as periodicity, thin film height, and refractive index. These analyses allowed rational design and optimization of the optical parameters and the device geometry.

RESULTS AND DISCUSSION

Finite element method was used to simulate the reflection and diffraction properties of SiO_2 based thin film gratings. Figure 1a shows the schematics of 400 and 500 nm thick SiO_2 thin film parallel gratings on Si substrate. Figure 1b shows a generic 2D computational geometry used to analyze the diffraction from these thin film gratings. The incident light was normal to the top of the SiO_2 thin film gratings. It was hypothesized that as the SiO_2 gratings became thicker, their diffraction spectrum

Received: April 24, 2017

DOI: 10.1021/acsphotonics.7b00419
ACS Photonics XXXX, XXX, XXX−XXX

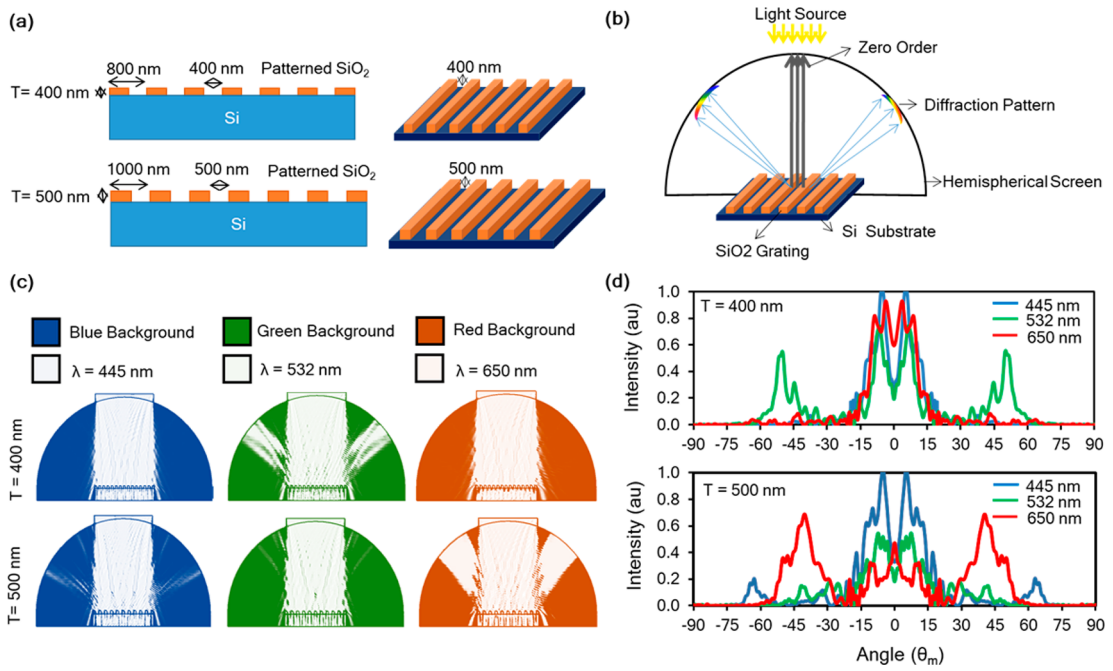

Figure 1. Simulations of 1D SiO_2 diffraction gratings. (a) SiO_2-based thin film gratings on Si, with 400 and 500 nm thicknesses (T). (b) Computational geometry for simulating optical diffraction. (c) Diffraction intensity analysis for 400 and 500 nm thick gratings in response to wavelengths (λ) 445 nm (blue), 532 nm (green), and 650 nm (red). (d) Diffraction patterns for 400 and 500 nm thick gratings showing high-intensity peaks for green and red light wavelengths, respectively.

red-shifted according to the thin film theory.[13,14] Figure1c,d demonstrates the computed reflected light intensity and the corresponding spectra for the 400 and 500 nm thick gratings in response to the 445 nm (blue), 532 nm (green), and 650 nm (red) incident light waves.

The far-field angular intensity profile from −90° to 90° was extracted from the computational domain to determine the zero, first, and second order intensities for each grating (Figure 1d). For higher diffraction orders, the angles of the maxima peaks and intensity profiles were studied; and for the zero order, diffraction intensities were analyzed. The theoretical diffraction angles (θ_m) displayed in Figure 1d were also calculated using the grating equation $d(\sin\alpha + \sin\beta) = m\lambda$, where α is the angle of incidence and β is the angle of reflected or diffracted light from the normal, d is the grating period, m is the diffraction order, and λ is the diffraction wavelength. The 400 nm thick grating showed a diffraction resonance for green light (Figure 1c,d). While the zero order consisted of high intensities of blue and green color, the first order was dominated by the green light. The thicker thin film grating (500 nm) preferentially diffracted red color as compared to the blue and green light. A pronounce red color is observed in the first order diffraction spectrum. The peaks observed were broad over the angles. This effect is due to the distance of the receiving boundary from the grating sample which was kept close in the near field to decrease the overall size of the geometry for fine simulation meshing. However, this broadness effect will not be observed at large distances in the far-field region. These results show that the thicknesses of thin films were vital in controling the diffraction wavelengths and by controlling the thicknesses wavelength selective diffractive structures can be achieved.

Further simulations were performed to analyze each of the thin-film grating parameters and their effects on the reflection and diffraction properties. Figure 2 displays the zero, first, and second order intensity plots for the simulated SiO_2 thin-film grating as a function of grating height (thin-film thickness) and period. Figure 2a–c show the zero order reflected intensity plots against the grating thicknesses, with each line showing the trend for a different grating periodicity. Similarly, Figure 2d–f, g, and h show the first and second order plots, respectively. It can be observed that each trend line on the plot shows a sinusoidal trend resonating at respective thicknesses, similar to that shown by thin films in reflection mode. In Figure 2a, it can be seen that for blue incident light (445 nm) almost all gratings are showing highest zero order reflection at thicknesses in the range of 450–500 nm. The level of intensity is observed to be decreasing with an increase in the period as this increases the diffraction of light to first and second orders instead of light being reflected back to zero order. Similar effect can be seen in Figure 2b and 2c (plots for green and red incident light) where the resonating thicknesses are around 400 and 470 nm, respectively. First order plots in Figure 2d–f also show the thin film resonance effect at thicknesses around 345, 400, and 500 nm for blue, green, and red wavelengths, respectively. The peaks observed in first (Figure 2d–f) and second (Figure 2g,h) orders are a result of both thin film and diffraction effect. Light diffraction is usually dependent on the ratio between the height (thickness) and the period of the grating for a particular wavelength, whereas thin film effect is dependent on thickness (height) and the change in refractive index with respect to the substrate. The grating heights at which the peak intensity peaks occurred for the first order were analogous to those of the zero order. This behavior can be observed in Figure 2a in which the gratings with high zero order blue reflection (thicknesses 450–550 nm) have low blue diffraction in first order (Figure 2d), whereas the result is opposite for the thicknesses 300–400 nm, which preferentially diffract blue color in the first order and low intensity peaks for the zero order. The zero order reflection is

DOI: 10.1021/acsphotonics.7b00419
ACS Photonics XXXX, XXX, XXX−XXX

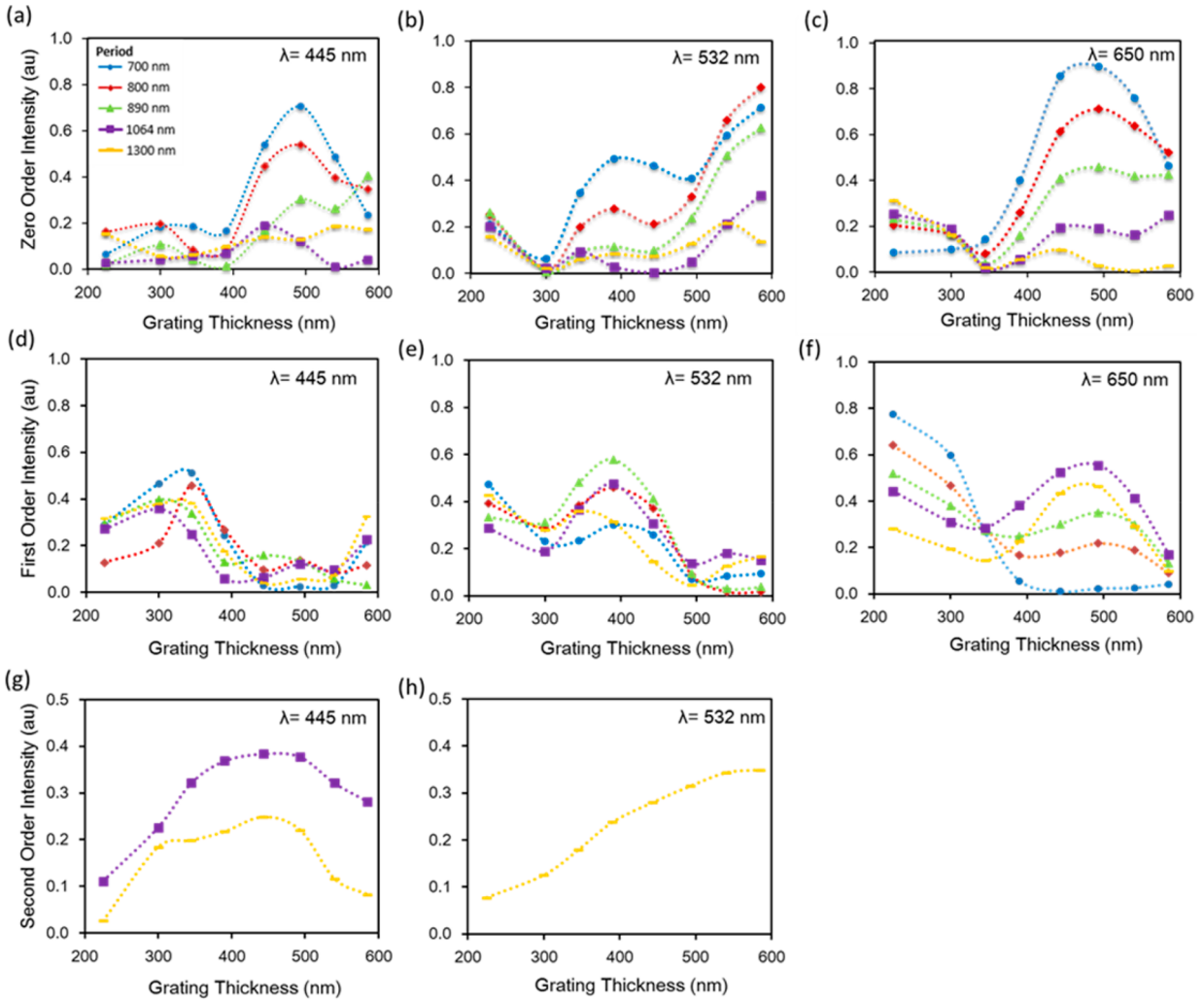

Figure 2. Simulations of the SiO_2 grating: (a–c) zero, (d–f) first, and (g, h) second order peak intensity plots with incident wavelengths of 445, 532, and 650 nm.

also periodicity dependent, as the grating with lowest period (700 nm) displays the highest zero order intensity peaks.

Another effect can also be analyzed by comparing green (532 nm) wavelength plots (Figure 2b,e), where zero order peak is observed at a thickness of 400 nm for a smaller period of 700 nm, while the first order peak for the same thickness occurs at a larger period of 900 nm. The same behavior is observed for red (650 nm) wavelength plots in Figure 2c,f, where resonance occurs at a thickness of 500 nm for both orders but at periodicities of 700 and 1064 nm, respectively. To summarize, it is observed that the grating periods and the behaviors of the peak maxima are correlated. As the period approached the same dimension as the examined incident wavelength, the original peak diverged into first and second order peaks showing the diffraction effect. This behavior is valid for the zero, first, and second order plots for the SiO_2 grating (Figure 2a–h). The phenomenon of peak splitting in periodic gratings has previously been observed for Bragg diffraction peaks due to the interference of asymmetric diffraction orders.[15,16]

Although diffraction was primarily investigated, zero and higher orders were analyzed showing specular reflection from the grating, but it was inherent to study the thin film thickness effect as the film thickness being the integral part of the grating feature had a major role in color selection of the diffracted light. Color charts for SiO_2 thin films are widely used (Figure S1) for thickness-based color selection, but to directly match the grating thickness with the corresponding thin-film thickness, the wavelengths being tested (445, 532, and 650 nm) have been simulated in MATLAB (Figure 3). Figure 3a displays the relative intensity of reflected polychromatic light for seven different thin-films of specific thickness and known reflective resonant color. The zero order peak intensity plots for the SiO_2 thin-film gratings in Figure 2a-c displayed a sinusoidal wave pattern which is analogous to the thin-film simulation plot in Figure 3b. For each wavelength simulated with the SiO_2 thin-film grating, the locations of the intensity peaks and troughs were consistent with the reflection spectra for SiO_2 uniform thin-films. For example, in Figure 3b, the observable thin-film interference occurred between 400 and 500 nm for the blue wavelength (445 nm), which is in accordance with the Figure 2a, where the resonating thickness existed between 400 and 500 nm for the same wavelength.

This was reinforced by the results in Figure 4 where the simulations were done purely on Si based gratings on a Si substrate. There is no change in refractive index of the grating and the substrate. The results displayed random behavior (Figure 4) showing no sign of thin film sinusoidal effect in comparison to the SiO_2 grating results in Figure 2. Zero order

DOI: 10.1021/acsphotonics.7b00419
ACS Photonics XXXX, XXX, XXX–XXX

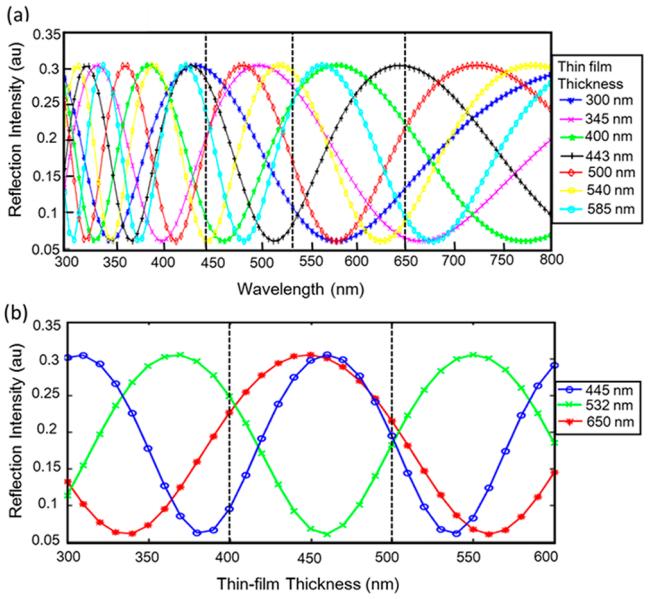

Figure 3. Reflection intensities of thin films as a function of (a) SiO_2 layer thickness and (b) film thicknesses for 445, 532, and 650 nm wavelengths.

intensity plots (Figure 4a–c) display a random behavior for blue, green and red wavelengths as compared to the sinusoidal zero orders seen for the SiO_2 gratings in Figure 2a–c, which were due to the difference in refractive index; and therefore, thin-film interference was present within the SiO_2 features. Similarly, the first order Si grating plots in Figure 4d–f display peaks, which were not correlated with Si layer thickness as compared to the SiO_2 grating plots in Figure 2d–f. Si grating plots demonstrate random behavior for all the orders where peak patterns exist at different locations for each grating period line (Figure 4), whereas SiO_2 peak intensity plots in Figure 2 follow a consistent pattern, with peaks and troughs were predominantly at the same location showing sinusoidal behavior for each grating period. The grating heights at which the peak intensity peaks occurred for the first order were analogous to those of the zero order (Figure 2), while no such behavior is observed in Figure 4. For example, in zero order (Figure 4a), high intensity peaks were visualized around 300 nm thickness for 700 and 900 nm periods, whereas the peaks appeared at thickness of 450 nm for 800, 1064, and 1300 nm periods for the same blue wavelength. Similarly, in first order (Figure 4d), high intensity peaks can be seen around 305, 320, 325, 345, and 450 nm thicknesses for the grating period of 800, 1300, 1064, 900, and 700 nm, respectively, for blue wavelength.

A SiO_2–Si grating has the same diffraction efficiency as that of a grating formed in Si–Si material, but has the advantage of having an ordered relationship between the grating feature dimensions and the intensity of reflected and diffracted wavelengths due to thin-film interference. Based on the simulation results, grating thicknesses of 400 and 500 nm

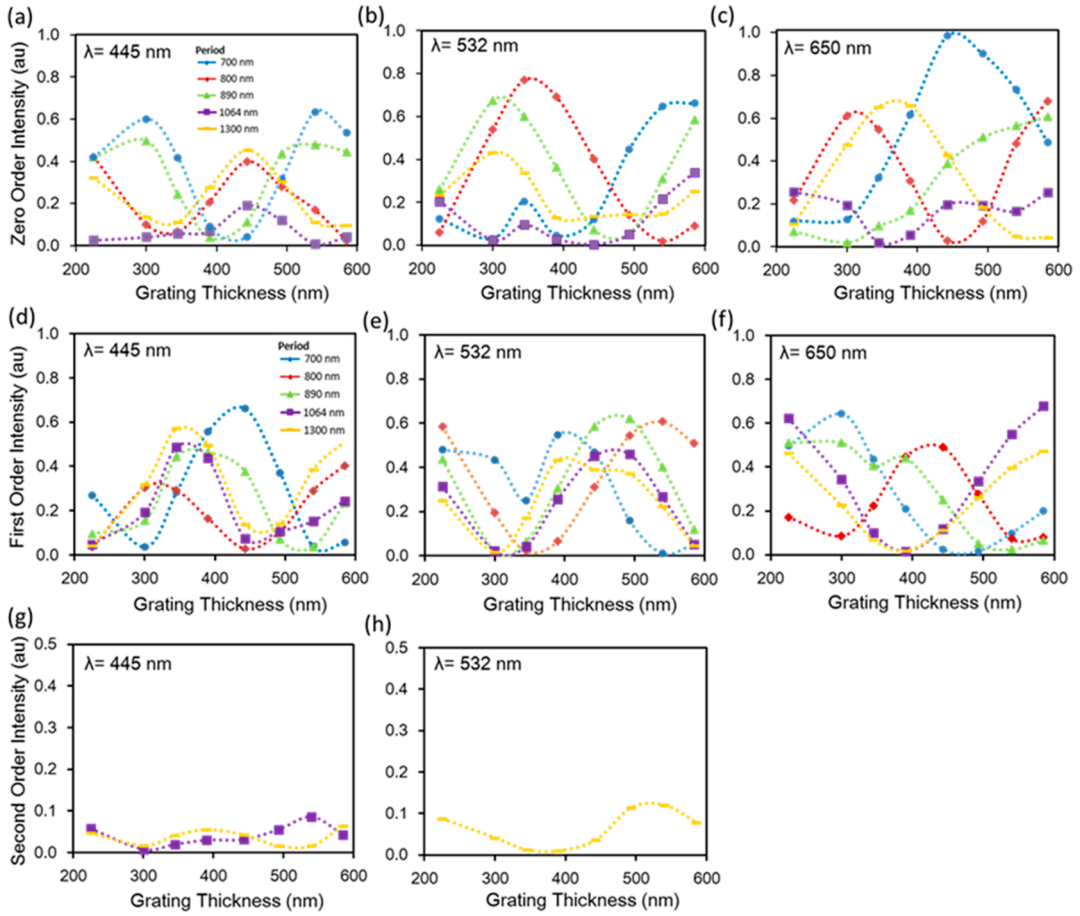

Figure 4. Simulations of Si gratings: (a–c) zero, (d–f) first, and (g, h) second-order peak intensity plots with incident wavelengths of 445, 532, and 650 nm.

DOI: 10.1021/acsphotonics.7b00419
ACS Photonics XXXX, XXX, XXX–XXX

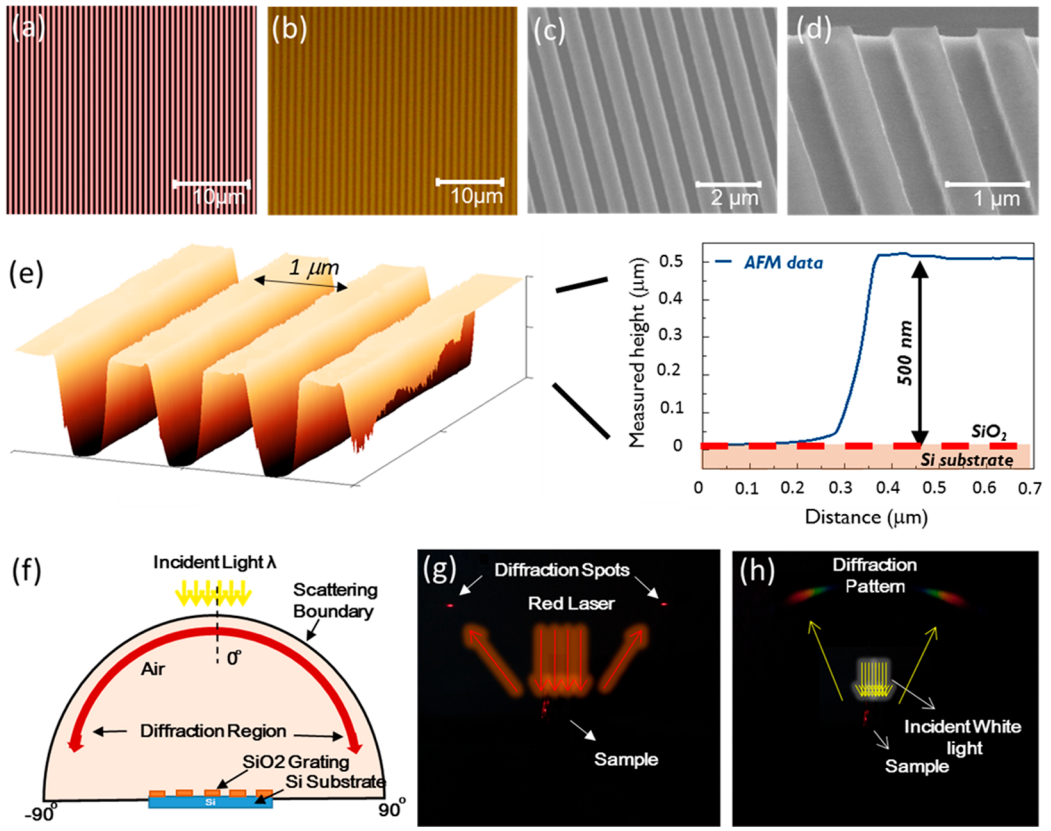

Figure 5. Optical characterization on SiO_2 gratings on a Si substrate. (a) Computer-Aided Design (CAD) mask of a grating having a periodicity of 500 nm. (b) Optical image of a 400 nm grating after e-beam lithography, etching, and resist cleaning. (c, d) SEM image of a 500 nm grating. (e) AFM image of a 500 nm grating. (f) Optical setup for the characterization of the diffraction grating. (g) Diffraction spots in reflection mode by shining red laser light perpendicular to the surface grating. (h) Diffraction pattern obtained by illuminating the grating with a broadband light in a semitransparent hemispherical screen.

with half periods of 400 and 500 nm were chosen to be fabricated. According to the results in Figure 2e,f, 400 nm grating should show the highest first order diffraction efficiency for green light, whereas 500 nm grating should show the highest diffraction efficiency for red light.

To fabricate the grating a Si wafer with thermally grown 400 nm (and later 500 nm) thick SiO_2 layer was used. The wafer was spin coated with UVIII resist. This resist allows both optical deep-UV lithography and electron beam lithography. Using a nanobeam setup, 400 nm (or 500 nm) strips were patterned over the substrate. The resist was developed with CD-26 solution to expose the SiO_2 surfaces, which are to be etched. A CHF_3 reactive ion beam etching step is carried to remove the SiO_2 down to Si wafer (as checked by atomic force microscopy (AFM)), while leaving the SiO_2 where it is protected by UVIII. After cleaning the structure in acetone to remove the resist, this process created desired diffraction pattern made of SiO_2 line array (millimeter long) over the Si substrate. Figure 6a–e demonstrates the optical, AFM, and scanning electron microscope (SEM) images of the fabricated gratings, respectively. AFM analysis in Figure 6e showed sharp edge profiles of the fabricated SiO_2 thin film gratings.

Figure 5f illustrates the experimental setup for the optical characterization of the grating. The diffraction pattern of the grating is shown in Figure 5g and h using monochromatic and broadband incident beams, respectively. A well-ordered rainbow was observed by using broadband light, where the red diffraction was at a higher angle and blue was at a lower angle (Figure 5h). For monochromatic laser incidence, the diffraction patterns were concentrated spots instead of broadband ribbons (Figure 5g). Diffracted spots in the reflection mode were visualized in backward direction by normal incident red laser light (Figure 5h).

The diffraction angles and efficiencies of the gratings for different monochromatic laser sources were studied by angle-resolved measurements. While standard wavelengths of 445, 532, and 650 nm were used in the simulated model, available laser beam wavelengths for the diffraction measurements were 403, 532, and 638 nm. The grating sample was illuminated normally on a rotation stage. Light intensity measurements were collected using a spectrophotometer at different angles with an angular resolution of 0.5°. Figure 6a–d shows the diffracted light intensity distribution in zero and first order for the three monochromatic light wavelengths. Blue and red wavelengths returned almost undiffracted to zero order for 400 nm grating (Figure 6a), whereas for 500 nm grating blue and green wavelengths dominate the zero order (Figure 6b). High diffraction of green light is observed in the first order (Figure 6c) for 400 nm grating, whereas red light is highly diffracted by the 500 nm grating (Figure 6d). The diffraction spots were visualized in the range of −90° to +90° with blue diffracted at lower angles compared to red. The diffraction angles for blue, green, and red light were measured to be 26°, 36°, and 44° for the 400 nm grating (Figure 6c) and 21°, 27°, and 34° for the 500 nm grating, respectively (Figure 6d). The variations in the diffraction angles in Figure 6c,d are due to the difference in

DOI: 10.1021/acsphotonics.7b00419
ACS Photonics XXXX, XXX, XXX−XXX

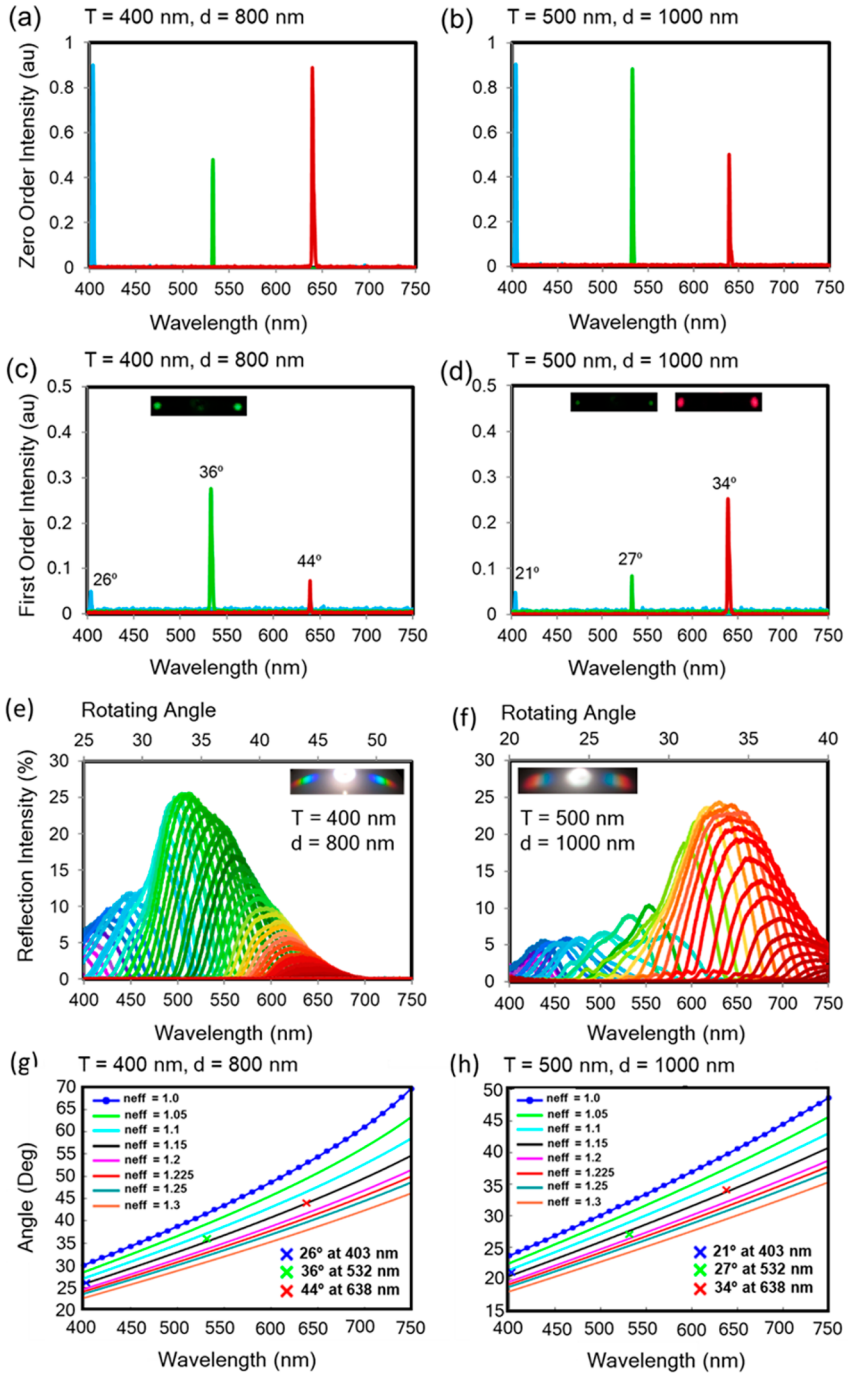

Figure 6. Optical characterization of the SiO_2 gratings. Zero order intensity distribution in response to 403, 532, and 638 nm wavelengths in reflection mode for (a) 400 nm (b) 500 nm thicknesses. (c) First order diffracted optical intensity distribution for 400 and (d) 500 nm grating. (e, f) Angle-resolved measurements of SiO_2 gratings. Specular first order reflection intensity distribution pattern in response to broadband light in reflection mode corresponding to rotational angles from 20° to 60° for 400 and 500 nm thick gratings. (g, h) Reduced diffraction angle plots with change in effective refractive index for 400 and 500 nm grating samples. Grating periods in (a, c, e, g) and (b, d, f, h) were 400 and 500 nm, respectively.

period and thickness of both grating samples. The difference between the analytical solution and the experimental results can be attributed to the thin film effect where the backscattered light constructively and destructively interferes to influence the location of diffraction spots. The diffraction efficiency for the incident blue, green and red lasers were experimentally measured to be 10% (blue), 56% (green), and 14% (red) for the 400 nm grating and 9% (blue), 16% (green), and 52% (red) for the 500 nm grating, respectively. Figure 6e,f shows the diffracted light intensity distribution for the first order in response to white broadband light. The broadband peaks (20−60°) were observed symmetrically from both sides of a central specular reflection spot (zero order), where the diffraction pattern was in agreement with Figure 5h. However, the diffraction peak angles observed were lower than those of grating equation. These angle differences were due to the thin film effect, where light undergoes refraction and reflection. A precise description of the angular position of the resolved peaks

DOI: 10.1021/acsphotonics.7b00419
ACS Photonics XXXX, XXX, XXX−XXX

was provided by using Bragg's law with effective refractive index terms:

$$n_{\text{eff}} \sin(\theta) = \frac{m\lambda}{d} \quad (1)$$

$$\lambda = \frac{d}{m} n_{\text{eff}} \sin(\theta) \quad (2)$$

where n_{eff} is the effective refractive index of the grating structure. It takes the reduced angle into account with respect to the normal at which light travels in the grating structure. For silica grating in air, it can be expressed as

$$n_{\text{eff}} = n_{\text{silica}} f_{\text{silica}} + n_{\text{air}} f_{\text{air}} \quad (3)$$

where $n_{\text{silica}} = 1.45$, $n_{\text{air}} = 1$, and f_{silica} and f_{air} are the volume fractions occupied by silica and air in the structure (generally 50% for a grating structure with equal dimensions). Hence, the theoretical value of n_{eff} was estimated as 1.225. Figure 6g,h shows the simulated plots for Bragg's law using MATLAB to evaluate the behavior of reduced diffraction angles with respect to change in refractive index for the two grating samples (400 and 500 nm). The measured values were near to the line representing $n_{\text{eff}} = 1.15$ resulting an inaccuracy of 6% based on the theoretical value of 1.225. This difference can be attributed to the real nonideal topology of the grating surface profile (Figure 5e). Stringent limitations in fabrication at nanoscale can affect the surface profile.[17] The experimentally measured values showed an agreement with the theoretical plots of reduced diffraction angle lines with respect to change in effective refractive index.

Light in a conventional reflection grating is diffracted from the top surface; however, in a thin film grating, the light is both diffracted (diffraction grating) and backscattered (thin film effect). The backscattered light undergoes coherent constructive and destructive interferences which has an overall effect on the reflection spectrum. The thin film grating of 400 nm periodicity and thickness displayed enhanced green spectrum in first order, ranging from 492 to 567 nm (Figure 6e). This is in agreement with the simulation results in Figures 1d and 2e. Similarly, as expected the 500 nm thin film grating displayed enhanced first order diffraction peaks in the red regime ranging from 595 to 725 nm (Figure 6f), which is in close proximity to the results in Figures 1d and 2f. These results were also in close agreement with the simulated results shown in Figure 2d–f and the thin film resonance plots shown in Figure 3b. Thus, the utilization of our simulation model allows creating gratings with predictable optical diffraction properties. The result supports the hypothesis that by optimizing the thin film grating features such as thickness, period, and refractive index, the optical properties can be tailored, especially to achieve color selective diffraction in first order.

CONCLUSION

SiO_2-based thin-film gratings obeyed the grating equation, displaying intensity maxima peaks in consistent locations even if the thin-film had variation in feature height. Due to thin-film interference, change in grating thickness resulted in the intensity of wavelengths regardless of the grating periodicity. However, the absolute value of diffraction intensity is dictated by the grating periodicity. The observed color of the grating was controlled separately from the diffraction maxima locations. The zero and first orders primarily displayed the same wavelengths, but as the intensity of the zero order increased with increasing grating height, the first order intensity decreased. These discernible investigations have led to a study of a new type of hierarchical grating that displayed optical properties which could be controlled independently. A grating with unique properties was created with predictable behavior such as desired optical bandwidth dictated by the grating features. It is anticipated that the designed grating will find applications in spectroscopy, biosensing, and security.

METHODS

Optical Characterization. The spectrophotometer (Ocean Optics 2000) with an optical resolution of ~0.1−100 nm fwhm was used to measure optical intensity with an integration time of 1 s to obtain the maximum peak intensity. COMSOL Multiphysics (V5.1) and MATLAB (MathWorks, V8.1) were used for finite element simulations and data processing.

ASSOCIATED CONTENT

Supporting Information

The Supporting Information is available free of charge on the ACS Publications website at DOI: 10.1021/acsphotonics.7b00419.

Silicon dioxide thin film color chart (PDF).

AUTHOR INFORMATION

Corresponding Author

*E-mail: h.butt@bham.ac.uk.

ORCID

Ali K. Yetisen: 0000-0003-0896-267X

Bruno Dlubak: 0000-0001-5696-8991

Notes

The authors declare no competing financial interest.

ACKNOWLEDGMENTS

H.B. thanks the Leverhulme Trust for the research funding.

REFERENCES

(1) Gaylord, T. K.; Moharam, M. Analysis and applications of optical diffraction by gratings. *Proc. IEEE* **1985**, *73*, 894−937.

(2) Vasconcellos, F.d.C.; Yetisen, A. K.; Montelongo, Y.; Butt, H.; Grigore, A.; Davidson, C. A. B.; Blyth, J.; Monteiro, M. J.; Wilkinson, T. D.; Lowe, C. R. Printable surface holograms via laser ablation. *ACS Photonics* **2014**, *1*, 489−495.

(3) Yetisen, A. K.; Butt, H.; Vasconcellos, F. D. C.; Montelongo, Y.; Davidson, C. A. B.; Blyth, J.; Chan, L.; Carmody, J. B.; Vignolini, S.; Steiner, U.; Baumberg, J. J.; Wilkinson, T. D.; Lowe, C. R. Light-Directed Writing of Chemically Tunable Narrow-Band Holographic Sensors. *Adv. Opt. Mater.* **2014**, *2*, 250−254.

(4) Palmer, C. A.; Loewen, E. G. *Diffraction Grating Handbook*; Richardson Grating Laboratory: New York, 2000.

(5) Won, K.; Palani, A.; Butt, H.; Hands, P. J. W.; Rajeskharan, R.; Dai, Q.; Khan, A. A.; Amaratunga, G. A. J.; Coles, H. J.; Wilkinson, T. D. Electrically Switchable Diffraction Grating Using a Hybrid Liquid Crystal and Carbon Nanotube-Based Nanophotonic Device. *Adv. Opt. Mater.* **2013**, *1*, 368−373.

(6) Butt, H.; Yetisen, A. K.; Mistry, D.; Khan, S. A.; Hassan, M. U.; Yun, S. Morpho Butterfly-Inspired Nanostructures. *Adv. Opt. Mater.* **2016**, *4*, 497.

(7) Du, X. M.; Almeida, R. M. Sintering kinetics of silica-titania sol-gel films on silicon wafers. *J. Mater. Res.* **1996**, *11*, 353−357.

(8) Brusatin, G.; Guglielmi, M.; Innocenzi, P.; Martucci, A.; Battaglin, G.; Pelli, S.; Righini, G. Microstructural and optical properties of sol-gel silica-titania waveguides. *J. Non-Cryst. Solids* **1997**, *220*, 202−209.

DOI: 10.1021/acsphotonics.7b00419
ACS Photonics XXXX, XXX, XXX−XXX

(9) Que, W.; Zhou, Y.; Lam, Y. L.; Chan, Y. C.; Cheng, S. D.; Sun, Z.; Kam, C. H. Microstructural and spectroscopic studies of sol-gel derived silica-titania waveguides. *J. Sol-Gel Sci. Technol.* **2000**, *18*, 77−83.
(10) Klimov, N. N.; Purdy, T.; Ahmed, Z. Fabrication and Characterization of On-Chip Integrated Silicon Photonic Bragg Grating and Photonic Crystal Cavity Thermometers. *arXiv preprint:1508.01419*, **2015**.
(11) Tsang, W. T.; Wang, S. Preferentially etched diffraction gratings in silicon. *J. Appl. Phys.* **1975**, *46*, 2163−2166.
(12) Perry, M.; Boyd, R. D.; Britten, J. A.; Decker, D.; Shore, B. W.; Shannon, C.; Shults, E. High-efficiency multilayer dielectric diffraction gratings: erratum. *Opt. Lett.* **1995**, *20*, 1513.
(13) Heavens, O. S. *Optical Properties of Thin Solid Films*; Courier Corporation, 1991.
(14) Pleil, M. W.; Plug and Play Microsystems (MEMS) Technology into an Engineering and Technology Program. *Proceedings of The 2014 IAJC/ISAM Joint International Conference ISBN 978-1-60643-379-9*, 2014.
(15) Tarnowski, K.; Urbanczyk, W. Origin of Bragg reflection peaks splitting in gratings fabricated using a multiple order phase mask. *Opt. Express* **2013**, *21*, 21800−21810.
(16) Guemes, J. A.; Menendez, J. M. Response of Bragg grating fiber-optic sensors when embedded in composite laminates. *Compos. Sci. Technol.* **2002**, *62*, 959−966.
(17) Montelongo, Y.; Tenorio-Pearl, J. O.; Williams, C.; Zhang, S.; Milne, W. I.; Wilkinson, T. D. Plasmonic nanoparticle scattering for color holograms. *Proc. Natl. Acad. Sci. U. S. A.* **2014**, *111*, 12679−83.

DOI: 10.1021/acsphotonics.7b00419
ACS Photonics XXXX, XXX, XXX−XXX